Excitation of quasielectrostatic waves in a laboratory magnetoplasma with weak spatial dispersion

Mikhail V. Starodubtsev,* Alexander V. Kostrov, Vladimir V. Nazarov, and German V. Permitin
Institute of Applied Physics, Russian Academy of Science, 46 Ulyanov Street, 603950 Nizhny Novgorod, Russia
(Received 5 April 2005; published 1 August 2005)

Short-wavelength quasielectrostatic waves radiated by a small probe in a cold ($T_e \approx 0.5$ eV) laboratory magnetoplasma are studied in both the upper-hybrid (UH) and the lower-hybrid (LH) frequency ranges. Measured radiation patterns are characterized by resonance cones in the LH range and in the low-frequency part of the UH range (at $\omega < 2\omega_c$), while in its high-frequency part (at $\omega > 2\omega_c$), a beamed radiation along the external magnetic field is observed. An analysis reveals that the angular resonance is primarily limited by the phase effects caused by weak spatial dispersion.

DOI: 10.1103/PhysRevE.72.026401 PACS number(s): 52.35.Fp, 52.35.Hr, 52.72.+v, 94.20.Bb

I. INTRODUCTION

Electrodynamic properties of magnetized plasmas in the so-called resonant frequency ranges [1] are characterized by significant growth of the refractive index n, when the angle φ between the wave vector $\mathbf{k}$ and the ambient magnetic field $\mathbf{B}_0$ approaches a critical value, φ_c. In a cold plasma without energy losses, n tends to infinity at φ_c, $n(\varphi \to \varphi_c) \to \infty$, while all components of the dielectric permittivity tensor $\varepsilon(\omega, \mathbf{k})$ behave regularly and monotonically. Using the analogy with usual frequency resonances, this effect could be interpreted as an *angular* resonance.

Angular resonances occupy two frequency ranges (if plasma ions are immobile), $\omega_{\mathrm{LH}} < \omega < \min(\omega_p, \omega_c)$ and $\max(\omega_p, \omega_c) < \omega < \omega_{\mathrm{UH}}$, where ω_p and ω_c are the plasma and the electron cyclotron frequencies, and ω_{LH} and ω_{UH} are the lower hybrid and the upper hybrid frequencies, respectively. Further we shall refer to these frequency ranges as the lower hybrid (LH) and the upper hybrid (UH) ones. Typical wave index surfaces in these domains are shown in Figs. 1 (LH range) and 2 (UH range) within the cold plasma approximation. Open wave index surfaces [Figs. 1(a) and 2(a)] form cones at large values of n [Figs. 1(b) and 2(b)]. Waves propagating along the cones are quasielectrostatic ($\mathbf{E} \| \mathbf{k}$); group velocities of these waves are orthogonal to their wave vectors and, due to the plasma axial symmetry, form a resonance cone with its opening angle $\theta_{\mathrm{res}} = \pi/2 - \varphi_c$. When dissipation is neglected, an elementary dipole radiates only in an infinitely narrow vicinity of the resonance-cone surface. In real physical systems, however, there are always factors that blur the resonance; such factors include collisional and collisionless energy dissipation, finite size of the emitter, plasma nonuniformity and unsteadiness, finite width of the radiation frequency spectrum, etc. If all these factors are small enough, then the radiation is concentrated within a small solid angle near the resonance (group) cone. Along all other directions, the energy transfer is not forbidden, generally speaking, but is suppressed by the angular resonance.

Emission of quasielectrostatic waves in the resonant frequency ranges has been studied by many authors [2–9]. Wave phenomena studied in laboratory conditions cover different issues, such as excitation of plasma resonance cones by antennas, electrodes, and electron beams [7,9], beam-plasma interaction [8], EM-ES mode conversion [10,11], etc. Quasielectrostatic waves are involved in different space plasma processes, such as auroral hisses [12,13], VLF triggered emissions [14], etc. Let us note separately ionospheric heating experiments [15–19], where an incident radiowave gives rise to plasma turbulence in the resonance region producing different wave phenomena such as stimulated electromagnetic emission (SEE) [16] and anomalous absorption of the radiowave [17,19]. The latter effect is related to the so-called thermal resonant instability [20–24] and develops, when quasielectrostatic UH plasma waves are trapped inside a small-scaled plasma density irregularity. Let us stress that this process is caused by weak spatial dispersion of iono-

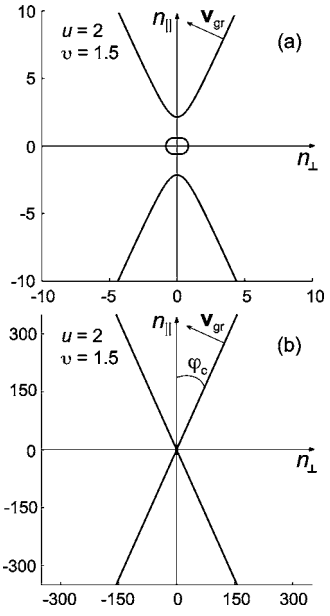

FIG. 1. Typical wave index surfaces ($n_\| = k_\|/k_0, n_\perp = k_\perp/k_0$) in the lower hybrid range calculated within the cold plasma approximation. The open wave index surface for the right-handed polarized (whistler) mode (a) form a cone with the opening angle φ_c (b). Group velocity $\mathbf{V}_{\mathrm{gr}}$ is perpendicular to the index surface.

*Electronic address: mstar@appl.sci-nnov.ru

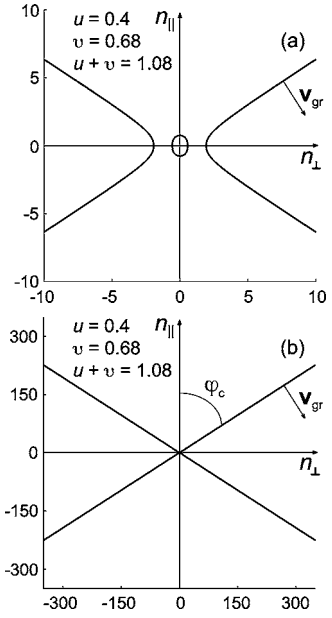

FIG. 2. Typical wave index surfaces ($n_{\|}=k_{\|}/k_0, n_{\perp}=k_{\perp}/k_0$) in the upper hybrid range calculated within the cold plasma approximation. The open wave index surface for the extraordinary mode (a) form a cone with the opening angle φ_c (b). Group velocity $\mathbf{V}_{\rm gr}$ is perpendicular to the index surface.

spheric plasma [21] due to its finite temperature. Namely, the thermal motion of plasma electrons modifies UH wave dispersion and causes a kind of short-wavelength electrostatic oscillation [1]. These oscillations are trapped and resonantly enhanced inside a density fluctuation, which leads to local Joule heating, plasma density modification and, finally, to plasma turbulence. This is an example of how the thermal motion of plasma electron modifies the dispersion of quasielectrostatic waves even at low plasma temperatures. As additional examples, we may refer to the beam-plasma discharges [25], Bernstein waves [26], etc.

Although thermal plasma waves are involved in different processes, ocurring both in natural plasmas and in applications, there is a rather small number of laboratory experiments studying their dispersion properties. Deformation of resonance cone structures due to plasma spatial dispersion and formation of oscillatory patterns in the field distribution of a small rf probe have been studied under some particular conditions [3,5,27]. However, the effect of thermal motion of plasma electrons on the dispersion of quasielectrostatic waves has not yet been characterized in laboratory experiment within the whole range of parameters, where these waves could exist. The present work deals with this objective. Our measurements cover an extremely wide parameter range and characterize quasielectrostatic waves as a function of plasma parameters in the whole UH and the main part of the LH ranges (we did not study only the lower-frequency part of the LH range, where the ion movement contributes to the wave dispersion, see Sec. II). We prevent also the excitation of electrostatic Bernstein waves (so-called the *h*-mode [5]) by adequate choise of emitter parameters. Hence, we deal only with the quasielectrostatic mode (the *m*-mode [5], which is shown in Figs. 1 and 2 for the cold plasma approximation). Our studies are limited by the case of weak spatial dispersion, when wave phase velocities V_{ph} are much greater than the electron thermal velocity V_{Te}: $V_{ph} \gg V_{Te}$. It is shown experimentally that even that weak spatial dispersion modifies the dispersion characteristics of UH quasielectrostatic waves significantly, while the characteristics of LH quasielectrostatic waves are still in good agreement with the cold plasma approximation. Dispersion properties of quasielectrostatic waves have been characterized as a function of plasma parameters; different domains have been revealed in the UH range depending on the influence of thermal correction.

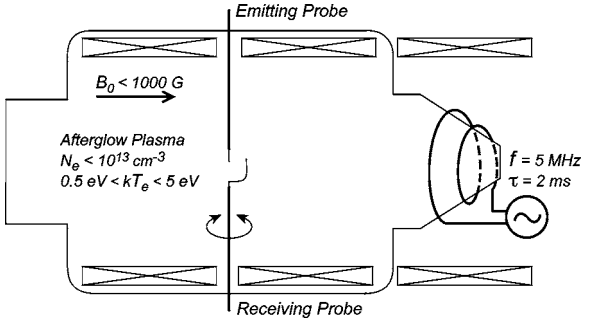

FIG. 3. Schematic of the experimental setup.

Our experimental approach is based on the examination of the precisely measured radiation patterns of a small electrostatically coupled antenna. Indeed, a small antenna excites a wide spectrum of wave vectors $\mathbf{k}$ with $k_{\max} \sim 1/R$, where R is the characteristic size of the antenna. Hence, analyzing the antenna radiation pattern we may describe qualitatively dispersion properties of waves with $k \lesssim k_{\max}$. If the open wave index surface forms an ideal cone [Figs. 1(b) and 2(b)] at such $\mathbf{k}$, the antenna will excite narrow resonance cones with their width approximately equal to the antenna size R (we neglect here all damping processes, see Sec. II). Any deformation of the wave index surface (caused, in our case, by thermal motion of plasma electrons) blurs the resonance cones and gives rise to the radiation propagating in nonresonant directions. Results of the laboratory measurements are compared with the calculated dispersion of quasielectrostatic waves with weak thermal corrections [1].

This paper is organized as follows: the experimental setup and conditions of the experiment are described in Sec. II; experimental results are presented in Sec. III and discussed in Sec. IV.

II. EXPERIMENTAL ARRANGEMENT

The experiment (see Fig. 3) is performed in a large laboratory plasma device (radius 70 cm, length 1.5 m). An axially magnetized ($B_0^{\max}=1000$ G), uniform, Maxwellian afterglow plasma column is produced in argon ($p=3\times10^{-3}$ Torr) with a pulsed inductive rf discharge (pulse duration $\tau_{\rm dis}=2$ ms, repetition rate $f_{\rm dis}=0.2$ Hz). Electron temperature kT_e is equal to 5 eV immediately after the end of the discharge pulse and reaches $kT_e \approx kT_i \approx 0.5$ eV in late afterglow. Electron-ion collisions dominate in dense plasma ($\nu_e \approx \nu_{ei}$

$\lesssim 10^8$ s^{-1}), while in rare plasma (at $n_e \lesssim 3\times 10^9$ cm^{-3}) electron-neutral collisions are more important ($\nu_e \approx \nu_{em} \approx 1.5\times 10^5$ s^{-1}). All measurements have been performed at low plasma densities 10^8 cm$^{-3} \lesssim n_e \lesssim 10^{10}$ cm^{-3}, when electron collision rate is small ($\nu_e < 3\times 10^5$ s^{-1}).

Wave characteristics have been studied at the center of the plasma column, where plasma density and the ambient magnetic field are highly uniform, $\Delta B_0/B_0 \lesssim 1\%$, $n_e/\nabla n_e \gtrsim 5$ m. Short-wavelength quasielectrostatic plasma eigenmodes are excited with a small insulated rf probe (length $l = 10$ mm, diameter $d = 1.5$ mm). Maximal wave numbers of the radiation are limited by the probe size, $k_{\max} \sim 1/d \sim 7$ cm^{-1}. A movable small noninsulated rf probe (length $l = 10$ mm, diameter $d = 0.5$ mm) is used to detect the radiation patterns of the emitter (Fig. 3). The distance between the emitter and the receiver is 8 cm.

Radiation patterns of the emitter have been studied in a wide range of plasma parameters,

$$10^7 \text{ cm}^{-3} < n_e < 10^{11} \text{ cm}^{-3}, \quad 30 \text{ G} < B_0 < 1000 \text{ G},$$

at signal frequencies 100 MHz $< f = \omega/2\pi < 3$ GHz. Using dimensionless parameters $u = \omega_c^2/\omega^2$ and $v = \omega_p^2/\omega^2$, we can represent the above parameter range as

$$0.05 < u < 100, \quad 0.01 < v < 100,$$

which naturally breaks into two resonant subranges, the upper hybrid,

$$0.05 < u < 1, \quad 1 - u < v < 1, \tag{1}$$

and the lower hybrid (or whistler),

$$1 < u < 100, \quad 1 < v \ll n_{\max}^2, \tag{2}$$

where $n_{\max} = k_{\max} c/\omega$ is the maximal refractive index produced by the emitting antenna. The latter inequality in (2) means that the emitter is well coupled to the quasielectrostatic branch of the whistler mode [9,28].

The characteristic parameter of spatial dispersion $\beta_{Te}^2 = (V_{Te}/c)^2$ (V_{Te} and c are the electron thermal velocity and velocity of light, respectively) was very small in the presented experiments, $\beta_{Te}^2 = 10^{-6}$.

The effect of the ambient magnetic field on the wave characteristics was essential, i.e., the inequality $k^2\rho_e^2 \ll 1$ (or $\beta_{Te}^2 n^2/u \ll 1$) has always been satisfied,

$$5\times 10^{-4} < k_{\max}^2 \rho_e^2 < 10^{-1}.$$

The damping processes did not influence the excitation of the resonance cones in this experiment. First, the parameter of collisional damping, ν/ω, was too small ($\nu/\omega \ll 10^{-4}$) to broaden the resonance [29]. The smallness condition for Landau damping ($\omega \gg k_{\max} V_{Te}$, or $\beta_{Te}^2 n_{\max}^2 \ll 1$) has always been satisfied due to low plasma temperature,

$$10^{-4} < \beta_{Te}^2 n_{\max}^2 < 10^{-2}.$$

Finally, to avoid the collisionless electron cyclotron damping we will not consider the close vicinity of the electron gyrofrequency: all measurements have been done out of the 30 MHz slot around f_c, where the damping is significant (the smallness condition for the electron cyclotron damping is $|\omega - \omega_c| \gg k_{\max} V_{Te} \approx 2\pi \times 30$ MHz).

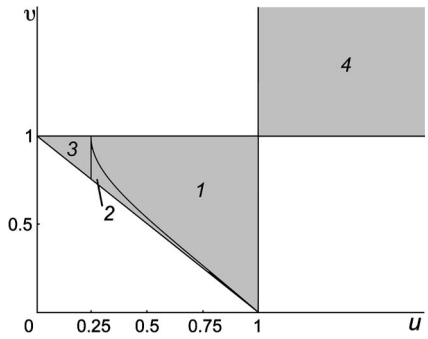

FIG. 4. Resonant frequency ranges, studied in our laboratory experiment. 1–3 is the upper hybrid range; 4 is the lower hybrid range. $v = \omega_p^2/\omega^2$, $u = \omega_c^2/\omega^2$. Different domains of the upper hybrid range are described in the text.

Thus, the measurements have been performed in a uniform, Maxwellian, collisionless, cold, afterglow laboratory magnetoplasma, when propagation of short-wavelength plasma waves are not distorted by dissipative processes. Present experiments were aimed at two main objectives, (i) to determine the parameter range, where the dispersion characteristics of quasielectrostatic waves conform to the cold plasma approximation, and (ii) to analyze how these characteristics are modified due to weak spatial dispersion of a laboratory magnetoplasma.

Measurements made at different frequencies (from 100 MHz to 3 GHz), densities (10^7 cm^{-3}–10^{11} cm^{-3}) and magnetic fields (30 G–1 kG) have clearly displayed that dispersion characteristics of the quasielectrostatic waves depend on the emitter frequency ω, plasma density n_e, and strength of the ambient magnetic field B_0 only in combinations ω_c^2/ω^2 and ω_p^2/ω^2. Thus, we will present our experimental results using dimensionless parameters $u = \omega_c^2/\omega^2$ and $v = \omega_p^2/\omega^2$ hereinafter. Parameter domains studied in the experiment are shown in Fig. 4 in the u-v plane. The upper hybrid range, which occupies a triangular area limited by the plasma resonance ($v = 1$), the cyclotron resonance ($u = 1$) and the upper hybrid resonance ($u + v = 1$) can be divided into three domains (Fig. 4). In domain 1 the dispersion properties of UH waves are determined by the angular resonances. This domain does not cover the entire upper hybrid range, as the parameters u and v decrease (domain 2), the angular resonance is suppressed; beamed radiation along the ambient magnetic field is observed in this case. No angular resonances are found also at frequencies above the second harmonic of the electron cyclotron frequency ($u < 0.25$, domain 3). Theoretical analysis has revealed the dominant mechanism for suppression of the angular resonance in our experiment, namely, the phase effects caused by weak spatial dispersion. This was not *a priori* evident because the characteristic parameter of spatial dispersion seemed to be negligibly small. Within the lower hybrid range (domain 4 in Fig. 4), pronounced angular resonances have always been observed, showing that plasma spatial dispersion does not modify the characteristics of LH quasielectrostatic waves. Let us remind that we studied only the high-frequency part

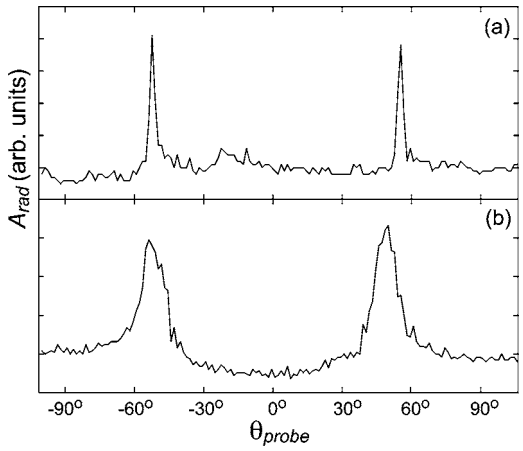

FIG. 5. Typical resonance cone structures measured, (a) in the lower hybrid range at $u \approx 2$, $\upsilon \approx 1.6$, and (b) in the upper hybrid range at $u \approx 0.7$, $\upsilon \approx 0.7$.

of the LH range ($\omega \gg \omega_{\mathrm{LH}}$), where the ion movement is negligible. Thus, we limited our studies by $u \lesssim 100$; higher u, when ion movement takes place, will be studied elsewhere.

III. EXPERIMENTAL RESULTS

Figure 5 represents typical resonance cones observed in the lower hybrid [Fig. 5(a)] and in the upper hybrid [Fig. 5(b)] domains. According to the estimations (Sec. II), resonance cones could not be broadened by collisional or collisionless damping, by plasma nonuniformity or unsteadiness. Formation of the resonance cones is limited only by the finite emitter size; thus, we should observe narrow cones with their characteristic width approximately equal to the probe diameter. However, one may notice that only LH cones [Fig. 5(a)] are in accordance with these speculation, while UH cones [Fig. 5(b)], are significantly wider than the expected value. Let us mention that both structures represented in Fig. 5 are measured at very close plasma parameters, hence, the difference between these two measurements is not caused by different experimental conditions.

One may also note that the damping processes as well as the effect of the finite antenna size should blur *both* the LH and UH resonance cones, which contradicts Fig. 5. The mechanism, which blurs only UH cones without affecting LH ones will be discussed in Sec. IV. This mechanism is, namely, associated with spatial dispersion of the laboratory plasma. Indeed, it has been shown that the cold plasma approximation is not sufficient to describe correctly dispersion properties of UH quasielectrostatic waves, which are significantly distorted by the thermal motion of plasma electrons. This conclusion is not evident, because the characteristic parameter of spatial dispersion, β_{Te}^2, is extremely small in our experiments ($\beta_{Te}^2 \sim 10^{-6}$, see Sec. II) and, consequently, plasma spatial dispersion is very weak.

Resonance cone structures measured at different $u = \omega_c^2/\omega^2$ are presented in Figs. 6 and 7 as a function of $\upsilon = \omega_p^2/\omega^2$. Figure 6 displays resonance cones in the LH range (i.e., at $u > 1$). Figures 6(b)–6(f) represent experimental results measured at the frequency $f = 300$ MHz, while Fig. 6(a) shows the position of LH resonance cones calculated within the cold plasma approximation for $u = 2$ [note a fairly good agreement between Fig. 6(a) and Fig. 6(c)]. As plasma density decreases, one may observe formation of the resonance cone structure in the field pattern of the emitter. In dense plasma (at $\upsilon > 10$), when electromagnetic effects takes place, the emitter excites preferentially quasilongitudinal whistlers propagating between the resonant directions. At lower densities ($\upsilon \sim 3$–10), pronounced maxima occurs in the vicinity of θ_{res}. Formation of the resonance cone structures is completed in rare plasma (at $\upsilon < 3$), when the emitting probe is well-coupled with the quasielectrostatic mode. In this regime one may observe extremely narrow resonance cones everywhere within the LH range (let us only remind that we do not consider here the lower-frequency part of the LH range with $u > 100$). Such pronounced angular resonances manifest that the LH index surface forms an ideal cone undisturbed by thermal effects. This ideal surface is extended up to wave indexes n greater then $n_{\max} = ck_{\max}/\omega$, i.e., up to $n > 100$ for Fig. 6.

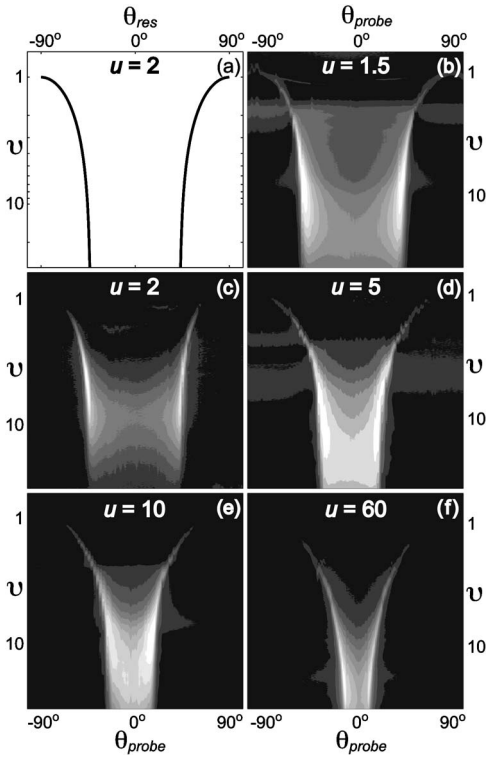

FIG. 6. Field patterns measured at different $u = \omega_c^2/\omega^2$ in the lower hybrid range as a function of $\upsilon = \omega_p^2/\omega^2$. (a) Position of cold resonance cones, (b)–(f) laboratory measurements.

Substantially different results are found when we examine the UH field patterns presented in Fig. 7. Here again, Fig. 7(a) represents the calculated positions of UH resonance cones, Figs. 7(b)–7(j) display the laboratory measurements. One may observe that at u close to unity [Fig. 7(b)] the measured field patterns correspond qualitatively to the cold plasma approximation. It means that only the resonance cone structure is detected within the whole UH range; no radiation in other directions is found. The single deviation from the

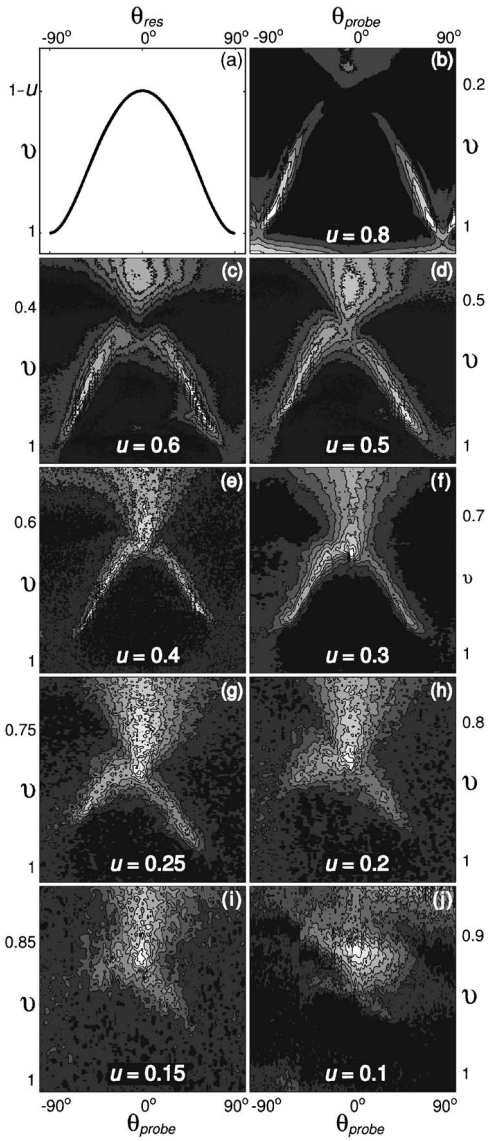

FIG. 7. Field patterns measured at different $u=\omega_c^2/\omega^2$ in the upper hybrid range as a function of $\upsilon=\omega_p^2/\omega^2$. (a) Position of cold resonance cones, (b)–(f) laboratory measurements.

cold plasma approximation reveals itself as an increased width of the UH cones, as it has been already discussed [compare also the width of resonance cones in Figs. 7(b)–7(f) with their width in Fig. 6 at $\upsilon\rightarrow 1$].

As $u=\omega_c^2/\omega^2$ decreases, the field pattern changes [Figs. 7(d)–7(g)]. This process occurs most strongly in the vicinity of the upper hybrid resonance (i.e., at $\upsilon\approx 1-u$). One may notice that the resonance cones merge when $\upsilon\rightarrow 1-u$ [compare Figs. 7(c) and 7(d) with Fig. 7(b)]. As a result, the position of resonance cones deviates from the cold approximation and the cones do not occupy the whole UH range anymore [compare Figs. 7(f) and 7(g) with Fig. 7(a)]. As ω approaches $2\omega_c$ [Figs. 7(e)–7(g)], modification of the field pattern in the vicinity of the upper hybrid resonance becomes even more pronounced, since a plasma eigenmode occurs as a narrow maximum at $\theta\approx 0$. Although its amplitude becomes greater than the amplitude of the resonance cones [Fig. 7(f)], the latter are still well observed. But when the frequency exceeds the doubled electron cyclotron frequency [Figs. 7(h)–7(j)], resonance cone stuctures disappear practically. The field pattern of the emitter is determined by the eigenmode in this case and represents a beamed radiation along the ambient magnetic field.

Summarizing these measurements, one may draw some rough conclusions about the dispersion characteristics of UH waves. First, angular resonances determine their dispersion at frequencies between ω_c and $2\omega_c$. Through the width of the resonance cones, we may estimate that the UH angular resonance is limited by $n=\sqrt{n_\parallel^2+n_\perp^2}\approx 15$ (compare with the LH resonance, which extends at least up to $n\approx 100$). At frequencies above the doubled electron cyclotron frequency, dispersion of UH waves does not exhibit pronounced angular resonances.

IV. DISCUSSION

The experimentally observed degeneration of the resonance cone structures, as well as formation of beamed radiation along the external magnetic field (i.e., within the shadow region in the cold plasma approximation) indicates that the Q factor of the angular resonance is limited, first of all, by weak kinetic effects, which deform the wave-vector surface. If energy dissipation is neglected, then the dispersion relation with weak thermal corrections takes on the following form [1]:

$$\delta n^6 + An^4 + Bn^2 + C = 0,$$

$$\delta = -\beta_{Te}^2 \upsilon [3(1-u)\cos^4\varphi + (6-3u+u^2) \times \sin^2\varphi\cos^2\varphi/(1-u)^2 + 3\sin^4\varphi/(1-4u)],$$

$$A = (1-u)(1-\upsilon)\cos^2\varphi - (u+\upsilon-1)\sin^2\varphi,$$

$$B = (u+\upsilon-1)(1-\upsilon)\cos^2\varphi + [\upsilon(1-\upsilon)+u+\upsilon-1]\sin^2\varphi,$$

$$C = -(1-\upsilon)[\upsilon(1-\upsilon)+u+\upsilon-1]. \quad (3)$$

Equation (3) is valid when

$$\frac{\beta_{Te}^2 n^2\cos^2\varphi}{(1-m\sqrt{u})^2} \ll 1, \quad (4)$$

which implies that collective losses of the wave energy are small [1]. Outside the cyclotron resonances at the harmonics of the electron gyrofrequency ($u=1, u=0.25$), condition (4) coincides practically with the requirement $kr_D \ll 1$, where r_D is the Debye radius.

When thermal corrections are neglected ($\delta=0$), Eq. (3) is reduced to the standard dispersion relation for cold plasma [1]. In such case, the highest term is proportional to n^4 and the equation describes two eigenmodes of the cold plasma. If A, the highest coefficient, tends to zero, then the refractive index of one of these eigenmodes (for the UH range, this is the extraordinary mode) tends to infinity ($A\rightarrow 0\Rightarrow n\rightarrow\infty$). This takes place at particular angle $\varphi=\varphi_c$,

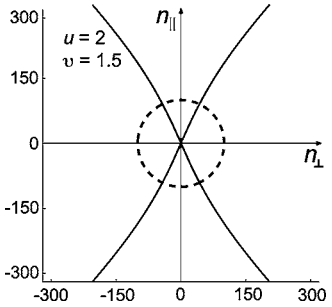

FIG. 8. Typical LH wave index surfaces ($n_\parallel = k_\parallel/k_0, n_\perp = k_\perp/k_0$) in a plasma with weak spatial dispersion ($T_e = 0.5$ eV). Dashed circle indicates the maximal refractive index $n_{\max}$, i.e., waves excited by the emitter lie mainly inside the circle.

$$\tan^2 \varphi_c = \frac{(1-u)(1-\upsilon)}{u+\upsilon-1}, \tag{5}$$

and, hence, the cold resonance cone occurs at $\theta_{\rm res} = \pi/2 - \varphi_c$.

If we consider thermal corrections in the form of Eq. (3), then the equation describes three dispersion branches. In the UH range, for example, these branches include ordinary waves (the thermal corrections to n_O are small, and we will not discuss them); extraordinary waves, which are modified in the vicinity of the angular resonance; and short-wavelength plasma waves. The refractive index of the latter waves n_p outside the cold resonant cone ($|A| \sim 1$) is approximately equal to $n_p \approx \sqrt{-A/\delta}$. Obviously, condition (4) in this case is not satisfied, and plasma waves are damped at distances of the order of their wavelength. The situation is different in the vicinity of the angular resonance, where $A \to 0$. In this case, we have $n_p \approx (B/\delta)^{1/4}$; i.e., $\beta_{Te}^2 n_p^2 \sim \beta_{Te} \ll 1$ and condition (4) is well satisfied. In the vicinity of the cold resonant cone, the extraordinary and plasma modes form a common weakly damped hybrid branch. The topology of this branch and, hence, the field pattern of an electrostatically coupled antenna depends substantially on the plasma parameters.

Figures 8–10 represent different types of wave index surfaces which arise in both the LH and UH ranges. Dashed circles indicate the characteristic value of maximal refractive index $n_{\max} = ck_{\max}/\omega \approx 100$. Analyzing the index surfaces, we should consider mainly those waves whose refractive indexes $n = \sqrt{n_\parallel^2 + n_\perp^2}$ lie incide the circle.

Within the LH frequency range, the electrostatic branch form, practically, only one type of index surfaces, which is displayed in Fig. 8. One may observe that the thermal effects modify only the perifery of the wave surface, while its central part (which we are especially interested in) remains unperturbed, in a perfect agreement with the laboratory measurements [see Fig. 5(a), Fig. 6].

The UH range is characterized by a more complicated topology of the electrostatic branch. According to its dispersion, the UH range divides into two subranges, $0.25 < u < 1$ and $u < 0.25$. Typical wave index surfaces in these subranges are presented in Fig. 9 ($0.25 < u < 1$) and Fig. 10 ($u < 0.25$). When the radiation frequency ω lies between the cyclotron

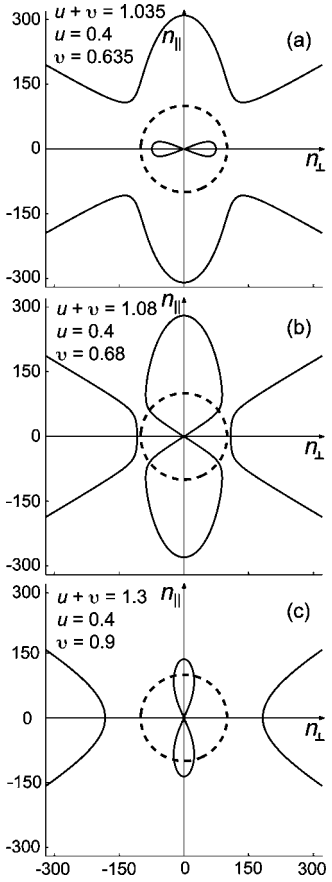

FIG. 9. UH wave index surfaces ($n_\parallel = k_\parallel/k_0, n_\perp = k_\perp/k_0$) in a plasma with weak spatial dispersion ($T_e = 0.5$ eV) at $0.25 < u < 1$. Dashed circles indicate the maximal refractive index $n_{\max}$, i.e., waves excited by the emitter lie mainly inside the circles.

frequency ω_c and its second harmonic $2\omega_c$ (Fig. 9), the cold resonance cone is transformed into two different types of index surfaces depending on plasma parameters. Namely, in the vicinity of the upper hybrid resonance [Fig. 9(a)] electrostatic waves form a toroidal index surface which turns into a dumbbell-shaped surface in the vicinity of the plasma resonance [Fig. 9(c)]. Note that in the transition region [Fig. 9(b)] the inner area of the index surface is characterized by very pronounced angular resonances and the field pattern of a small antenna should represent well-formed resonance cones [compare with Figs. 7(b)–7(f)]. Hence, in the parameter range

$$0.25 < u < 1, \quad 1 - u < \upsilon < 1 \tag{6}$$

(Fig. 4, domain 1), kinetic processes do not destroy the resonant cones completely. However, these processes limit the width of the angular resonance and, as a result, the singularity at $\theta = \theta_{\rm res}$ become integrable, i.e., the power emitted along the resonant cone is finite. The solid angle where this power is concentrated decreases with distance as $\Delta\Omega \propto 1/r^{1/3}$.

Comparing the experimentally measured resonance cones [Figs. 7(b)–7(g)] and the angular resonances observed in Fig. 9, one should notice an interesting discrepancy. Indeed, the characteristic width of the UH resonance cones is measured

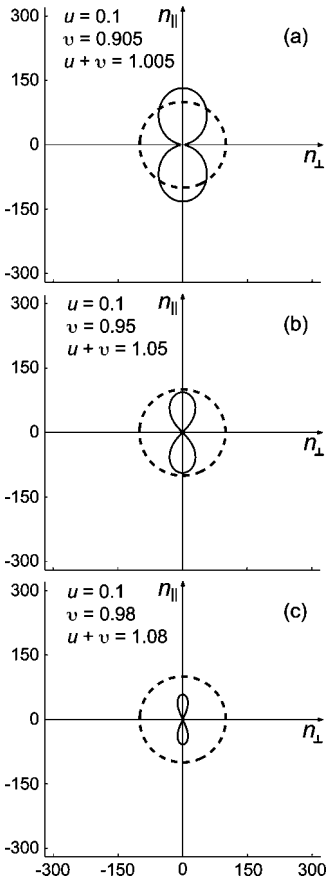

FIG. 10. UH wave index surfaces ($n_\parallel = k_\parallel/k_0, n_\perp = k_\perp/k_0$) in a plasma with weak spatial dispersion ($T_e = 0.5$ eV) at $u < 0.25$. Dashed circles indicate the maximal refractive index $n_{\max}$, i.e., waves excited by the emitter lie mainly inside the circles.

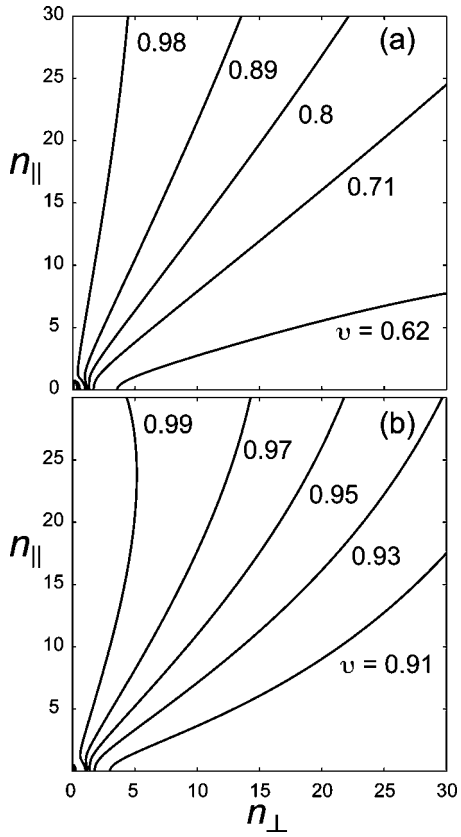

FIG. 11. Large-scale plot of UH wave index surfaces. (a) $u = 0.4$, (b) $u = 0.1$.

to be of the order of 0.7 cm and remains practically constant within the whole range (6). This fact contradicts to Fig. 9, where the extention of angular resonances changes substantially [compare Figs. 9(a)and 9(c) with Fig. 9(b)].

One interesting property of the UH electrostatic branch at $0.25 < u < 1$ is connected with toroidal wave index surfaces, which are shown in Fig. 9(a). A characteristic feature of such surfaces is the presence of modes of internal conical refraction, the entire wave-vector cone corresponds to the same direction of the group velocity, specifically, the direction along the magnetic field. The amplitude of the conical-refraction mode decreases with distance from the source as $1/\sqrt{r}$, and its transverse field structure is described with a Bessel function [30]. This eigenmode forms a singularity in the field pattern of a small emitter, which may be used to explain the narrow radiation maximum at $\upsilon \gtrsim 1-u$ observed in Figs. 7(e) and 7(f).

Another specific feature of the conical-refraction mode, which makes it an interesting object for inquiry, is that its group velocity is directed oppositely to the wave vector; i.e., this mode is a backward wave. Since this wave is slow, it can be easily excited by an electron beam whose velocity is somewhat higher than the wave phase velocity. Probably, a sort of such a backward-wave tube can operate in the Earth ionosphere and magnetosphere. However, to assert this with certainty, it is necessary to perform calculations of the threshold currents and carry out relevant laboratory experiments.

Topology of the UH electrostatic branch at frequencies above the doubled electron cyclotron frequency (Fig. 10) is qualitatively different. It always forms a dumbbell-shaped index surface and pronounced angular resonances do not occur. Moreover, deformation of the electrostatic branch starts at very small n. This fact is clearly seen in Fig. 11, which displays the inner parts of the UH index surfaces for $0.25 < u = 0.4 < 1$ [Fig. 11(a)] and for $u = 0.1 < 0.25$ [Fig. 11(b)]. One may observe that thermal effects cause the deformation of angular resonances at much smaller n in the latter case. Thus, this result may explain qualitatively the disappearence of resonance cone structures, which has been observed in laboratory experiment at $\omega > 2\omega_c$ [Figs. 7(h)–7(j)]. Let us also notice that the nature of the beamed radiation along the ambient magnetic field detected in this frequency domain is not evident from Fig. 10; detailed analysis of this eigenmode requires further experimental and theoretical studies.

V. CONCLUSIONS

Excitation of quasielectrostatic waves has been studied in a low-temperature laboratory plasma in the lower hybrid and the upper hybrid frequency ranges. Excitation of plasma resonance cones have been evidenced in both ranges. The

lower hybrid cones are found to be in a good agreement with the cold plasma approximation, while the upper hybrid ones are significantly influenced by the weak spatial dispersion. The parameter domain where the UH cones are detected and the properties of UH angular resonances differ significantly from the cold plasma approximation. Different parameter domains within the UH range have been revealed depending on the effect of weak spatial dispersion.

(i) At $\omega_c \lesssim \omega < 2\omega_c$, weak spatial dispersion limits the width of the angular resonance, but the resonance cones remain well pronounced.

(ii) As $\omega \to 2\omega_c$ weak spatial dispersion results in the degeneration of the UH resonance cones; at $\omega > 2\omega_c$ no resonance cone structure is observed.

In the latter case, however, a UH electrostatic eigenmode propagating along the ambient magnetic field is efficiently excited. To recover the nature of this mode, further experimental and theoretical studies are required.

The experimental results presented in this paper can be used to develop active satellite diagnostics of the near-Earth plasma and reveal the mechanisms for generation of high-frequency ionospheric noise and plasma turbulence.

ACKNOWLEDGMENTS

This work is supported by the Russian Foundation for Basic Research (Grant No. 04-02-17105), grants of the President of Russian Federation for Young Candidates of Science (Grant No. 4355.2004.2) and for Leading Scientific Schools (Grant No. 1639.2003.02), grants of the Presidium RAS and the Russian Science Support Foundation.

[1] V. L. Ginzburg, *The Properties of Electromagnetic Waves in Plasmas* (Pergamon, New York, 1964).
[2] R. K. Fisher and R. W. Gould, Phys. Rev. Lett. **22**, 1093 (1969).
[3] U. Kortshagen and A. Piel, Phys. Fluids B **1**, 538 (1989).
[4] P. Bellan and K. Wong, Phys. Fluids **21**, 592 (1978).
[5] T. Pierre and G. Leclert, Plasma Phys. Controlled Fusion **31**, 371 (1989).
[6] R. Stenzel and W. Gekelman, Phys. Fluids **20**, 108 (1977).
[7] M. Starodubtsev, C. Krafft, P. Thevenet, and A. Kostrov, Phys. Plasmas **6**, 1427 (1999).
[8] M. Starodubtsev and C. Krafft, Phys. Plasmas **6**, 2598 (1999).
[9] M. Starodubtsev and C. Krafft, J. Plasma Phys. **63**, 285 (2000).
[10] R. Ellis, G. Tsakiris, C. Wang, and D. Boyd, Plasma Phys. Controlled Fusion **28**, 327 (1986).
[11] T. Intrator, N. Hershkowitz, and C. Chan, Phys. Fluids **27**, 527 (1984).
[12] E. Bering, J. Maggs, and H. Anderson, J. Geophys. Res., [Atmos.] **92**, 7581 (1987).
[13] R. Stenzel, J. Geophys. Res. **82**, 4805 (1977).
[14] Y. Omura, D. Nunn, H. Matsumoto, and M. Rycroft, J. Atmos. Terr. Phys. **53**, 351 (1991).
[15] B. Thidé, H. Kopka, and P. Stubbe, Phys. Rev. Lett. **49**, 1561 (1982).
[16] P. Stubbe, H. Kopka, B. Thidé, and H. Derblom, J. Geophys. Res., [Atmos.] **89**, 7523 (1984).
[17] P. Stubbe, A. Stocker, F. Honary, T. Robinson, and T. Jones, J. Geophys. Res., [Atmos.] **99**, 6233 (1994).
[18] P. Stubbe, J. Atmos. Terr. Phys. **58**, 349 (1996).
[19] A. Stocker, F. Honary, T. Robinson, T. Jones, and P. Stubbe, J. Geophys. Res., [Atmos.] **98**, 13627 (1993).
[20] K. Dysthe, E. Mjølhus, H. Pecseli, and K. Rypdal, Phys. Scr., T **T2/2**, 548 (1982).
[21] V. Vas'kov and A. Gurevich, Geomagn. Aeron. **24**, 350 (1984).
[22] A. V. Gurevich, K. P. Zybin, and A. V. Lukyanov, Phys. Rev. Lett. **75**, 2622 (1995).
[23] E. Mjølhus, J. Atmos. Terr. Phys. **55**, 9907 (1993).
[24] E. Mjølhus, J. Plasma Phys. **58**, 747 (1997).
[25] R. Boswell, I. Morey, and R. Porteous, J. Geophys. Res., [Atmos.] **94**, 2654 (1989).
[26] J. Thiel and B. Lembège, Phys. Fluids **25**, 551 (1982).
[27] R. K. Fisher and R. W. Gould, Phys. Fluids **14**, 857 (1971).
[28] R. L. Stenzel, Radio Sci. **11**, 1045 (1976).
[29] K. Lucks and M. Kramer, Phys. Fluids B **22**, 879 (1980).
[30] L. Felsen and N. Marcuvitz, *Radiation and Scattering of Waves* (Prentice-Hall, Englewood Cliffs, NJ 1973).